Supplementary Information for

First-principles high-throughput screening of ruthenium compounds for advanced interconnects

Gyungho Maeng,[a] Subeen Lim,[a] Bonggeun Shong,[b] and Yeonghun Lee*[ac]

[a] *Department of Electronics Engineering, Incheon National University, Yeonsu-gu, Incheon 22012, Republic of Korea.*
[b] *Major in Advanced Materials and Semiconductor Engineering, Hanyang University, Ansan-si, Gyeonggi-do 15588, South Korea.*
[c] *Research Institute for Engineering and Technology, Incheon National University, Yeonsu-gu, Incheon 22012, Republic of Korea.*

* Corresponding author.
E-mail address: y.lee@inu.ac.kr (Y. Lee).

1. Resistivity-based averaging scheme

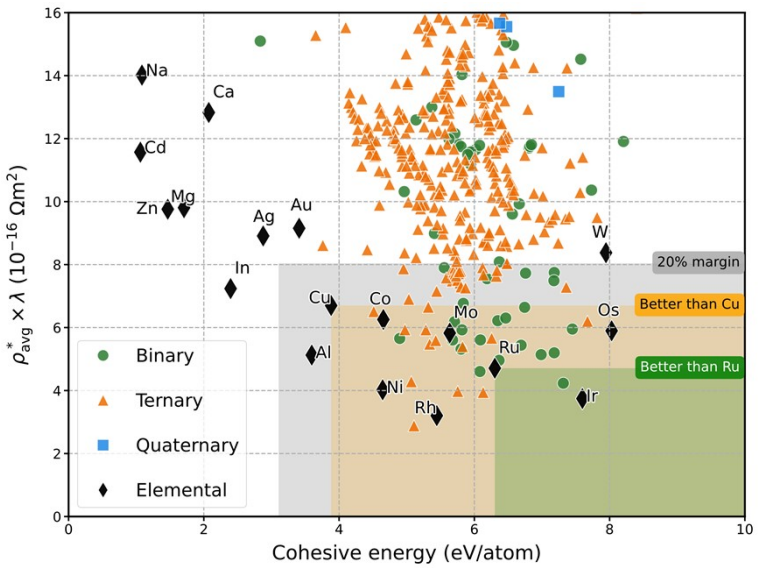

Fig. S1. Global screening results using the resistivity-based averaging scheme. The electrical properties ($\rho^*_{avg} \times \lambda$) are plotted as a function of cohesive energy for all screened Ru-based compounds. This plot serves as the resistivity-based counterpart to Fig. 2 in the manuscript. The shaded areas represent the performance margins relative to Cu and Ru. Note that due to the inclusion of high-resistivity direction in the averaging, some anisotropic compounds may exhibit inferior resistivity performance compared to the conductivity-based results.

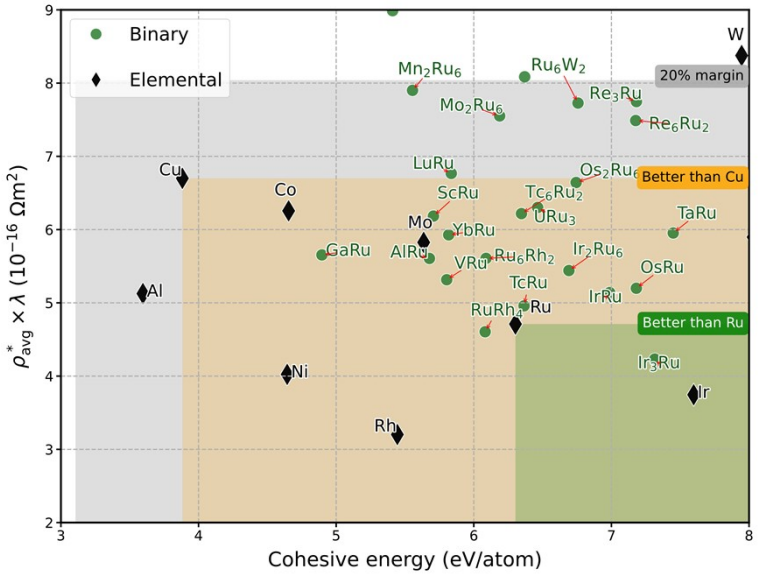

Fig. S2. Evaluation of binary Ru compounds based on the resistivity-based metric. The scatter plot displays the distribution of binary candidates against the Cu and Ru benchmarks. This corresponds to Fig. 3 in the manuscript. Notably, the binary compound Tc_2Ru_6 falls outside the promising window in this plot due to the increased average resistivity resulting from its anisotropic transport properties. Consequently, under this upper-bound estimation, the number of promising binary candidates is slightly reduced from 23 to 22.

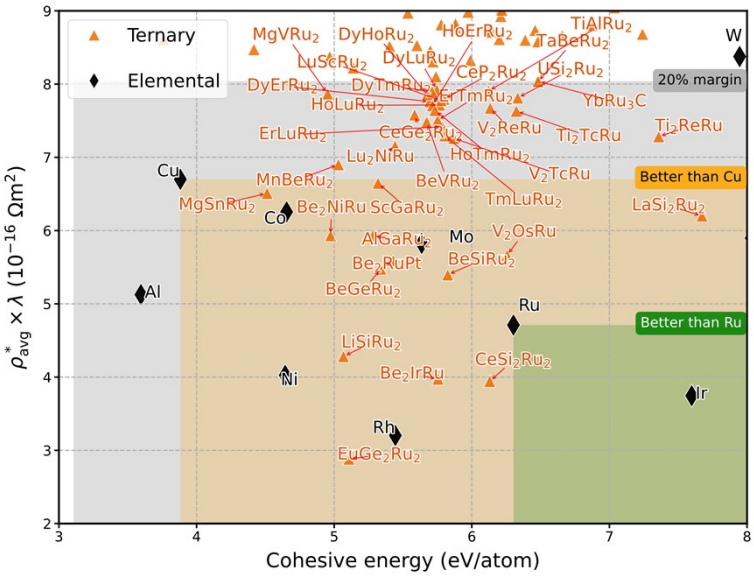

Fig. S3. Evaluation of ternary Ru compounds based on the resistivity-based metric. The distribution of ternary candidates is mapped across the performance-stability design space. This corresponds to Fig. 4 in the manuscript. While the total number of promising ternary candidates remains unchanged compared to the conductivity-based scheme, the specific transport properties for six anisotropic compounds are adjusted upward. This shift visually reflects the impact of directional anisotropy when evaluating the theoretical upper limit of resistivity.

As detailed in the manuscript, the primary screening utilized a conductivity-based averaging scheme ($\rho_{avg} \times \lambda$), assuming an effective medium where current flows through multiple crystallographic channels simultaneously. In contrast, this section presents the screening results based on the resistivity-based averaging scheme ($\rho^*_{avg} \times \lambda$), which mimics extreme confinement in narrow interconnects where directional resistances are effectively combined in series. Consequently, this metric highlights the influence of high-resistivity directions and provides a theoretical upper bound on the electrical resistivity. Comparing the results in Figs. S1-S3 with those in the main text (Figs. 2-4), distinct numerical shifts are observed for non-cubic compounds exhibiting strong anisotropy, verifying the performance variation due to directional sensitivity.

2. Expanded display of elemental metals

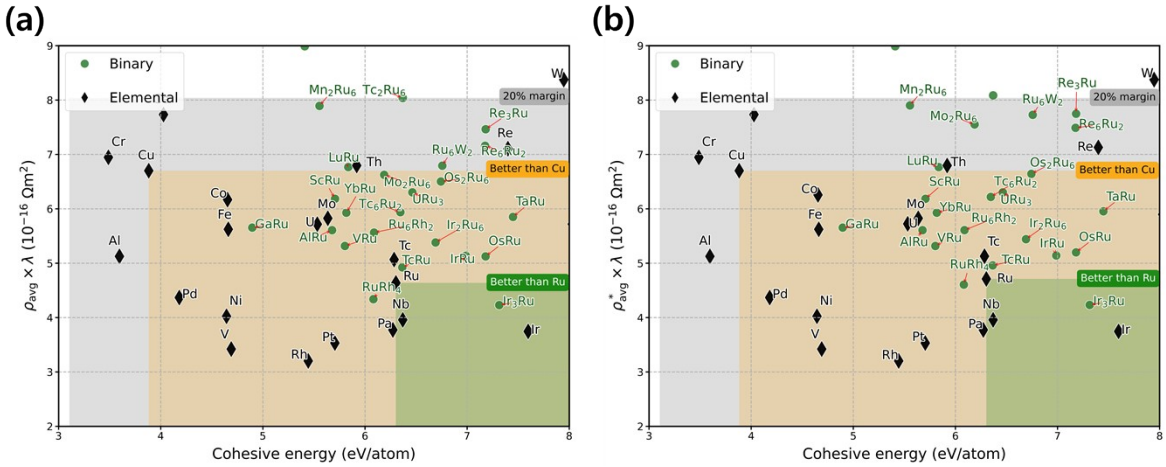

Fig. S4. Binary Ru compounds with expanded metallic elements based on the (a) conductivity-based average and (b) resistivity-based average metrics. Elemental metals (black diamonds) are plotted alongside the screened binary compounds (green circles).

The plots display $\rho_{avg} \times \lambda$ versus cohesive energy (E_{coh}) evaluated via the (a) conductivity-averaged and (b) resistivity-averaged schemes. This expanded analysis visually demonstrates that the performance metrics of a compound typically interpolate between those of its elemental constituents or degrade further. This supports the conclusion that compound formation fundamentally redistributes, rather than inherently transcends, the intrinsic electronic properties of the pure building blocks.

3. Compositional descriptors extracted via the XenonPy toolkit

Table S 1 List of top 10 elements-level compositional features from XenonPy

Compositional property	Description
vdw_radius_uff	Van der Waals radius from the UFF
melting_point	Melting point
heat_of_formation	Heat of formation
evaporation_heat	Evaporation heat
fusion_enthalpy	Fusion heat
hhi_r	Herfindahl-Hirschman Index (HHI) reserves values
num_s_unfilled	Unfilled electron in s shell
num_p_unfilied	Unfilled electron in p shell
gs_energy	DFT energy per atom (raw VASP value) of $T = 0$ K ground state
gs_est_bcc_latcnt	Estimated BCC lattice parameter based on the DFT volume
gs_est_fcc_latcnt	Estimated FCC lattice parameter based on the DFT volume
gs_volume_per	DFT volume per atom of $T = 0$ K ground state
Bulk_modulus	

These properties represent the variance of elemental features within each compound and were identified through Pearson correlation analysis as having the strongest relationships with the intrinsic transport metric.